RF Interferometer Concept
with
Baseline Geometry and Frequency Scaling

R. Alan Conrad
microwaves@att.net

A Spreadsheet-Driven Method for Visualizing DOA Accuracy and Baseline Behavior in Three- and Four-Channel RF Interferometers

1. Introduction

NRL Report 8005 (September 1976) by Robert L. Goodwin established the analytical foundation for RF interferometer arrays, providing the first coherent treatment of the basic theory and synthesizing four-element, three-integer-set geometries. Much of the modern interferometer design lineage traces directly to this work. Goodwin's report addressed the practical engineering problems of interferometer systems, quantified channel-to-channel phase-tracking errors, demonstrated how they degrade DF accuracy, and presented block diagrams from RF input through ambiguity removal and angle computation. No other source of the period provided comparable system-level clarity.

This historical framework enables a modern, spreadsheet-driven approach. By expressing the four-antenna spacing geometry, the interferometer phase equation, and the physical separations between array elements directly in Excel, the DOA and unwrapped-phase functions can be computed in a fully transparent form. The entire system can be visualized, tested, and modified without specialized software. All calculations use the Hybrid Mid-Phase Array, with Channel 2 serving as the reference channel.

2. Hybrid Mid-Phase Geometry (Channel 2 Reference)

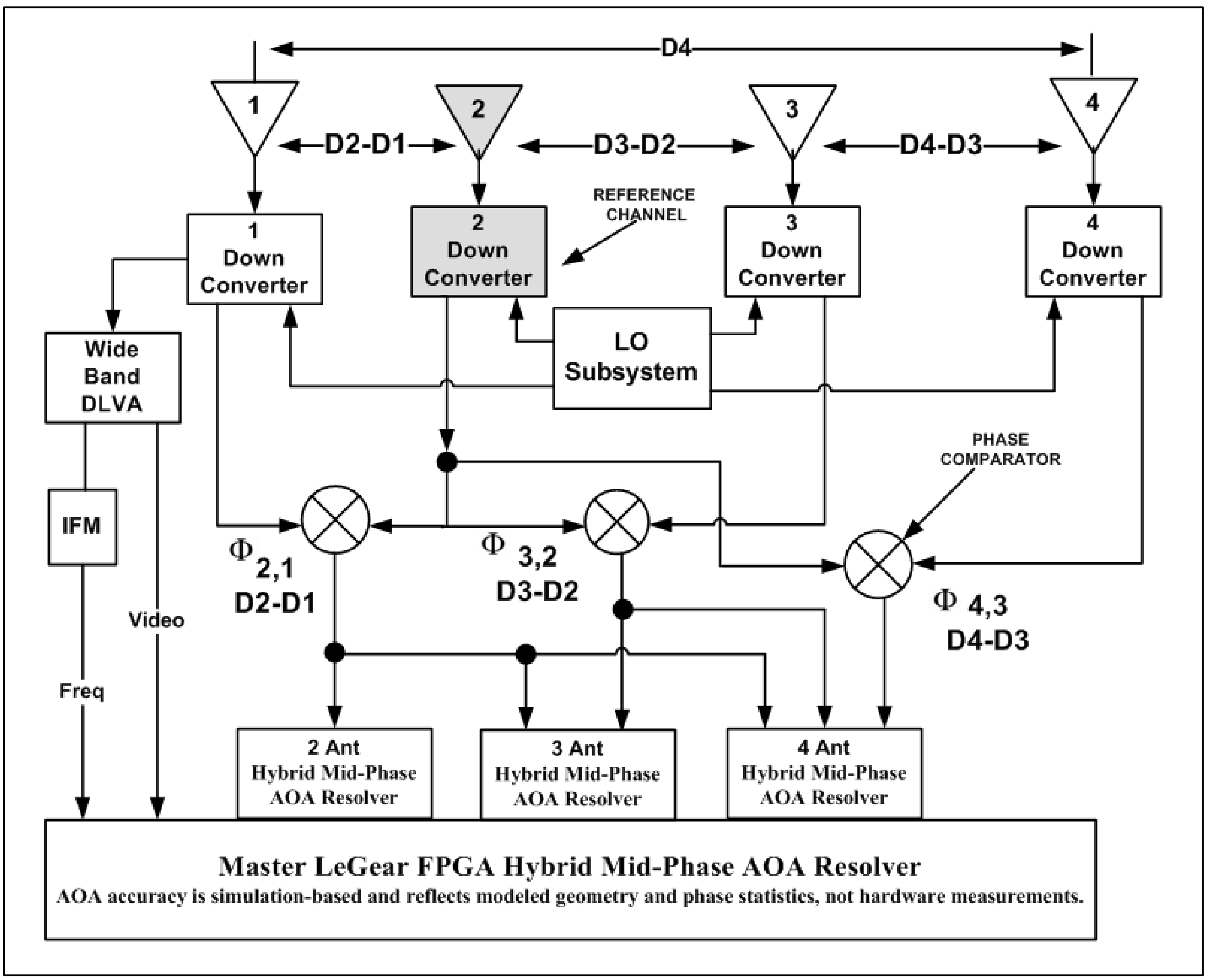

Figure 1 Hybrid Mid-Phase Geometry

The Hybrid Mid-Phase geometry is the compact, reference-centered configuration used for all DOA calculations in the worksheet. In this arrangement, Channel 2 serves as the reference antenna, and the effective baselines are formed by subtracting adjacent physical spacings. This hybridization produces the smallest effective four-element structure, even though the physical antenna positions remain unchanged.

The physical array consists of antennas D1, D2, D3, and D4 arranged along a straight line. The hybrid mid-phase formulation replaces the raw cumulative spacings with the reduced hybrid baselines P, Q, and R, and the absolute baseline S. These hybrid baselines are electrically smaller because they represent differences between adjacent spacings rather than the full end-to-end separations. As a result, the effective electrical aperture is centered on Channel 2, and the phase slopes remain manageable across the field of view.

Figure 2 shows the D2 reference antenna and the resulting spacings D1, D2, D3, and D4, with spacings D2-D1, D3-D2, and D4-D3 used in the worksheet. The diagram provides the physical baseline layout corresponding to the P, Q, R, and S phase-difference columns. These geometric definitions drive the unwrapped phase calculations and establish the effective baseline relationships used throughout the system.

The Hybrid Mid-Phase geometry reduces wrap density at higher frequencies and maintains clear baseline separation across the operating band. This compact effective structure is why the mid-phase configuration is used for all visualizations and DF accuracy curves in the spreadsheet.

3. Antenna Baseline Spacing Calculator

λ (Inches)	Design Anchor	D1(P)	D2(Q)	D3(R)	D4(S)S
0.656	18 GHz	4.000	6.000	11.000	21.000
Freq GHz	Scale Factor	P (λ/2)	Q (λ/2)	R (λ/2)	S 2(λ/2)
18.000	4.300	2.000	3.000	5.500	10.500
	Phase Scaling λ/2	19.156	28.734	52.679	100.569
	Befor Scaling	4.455	6.682	12.251	23.388
	Array Scale Factor	D2-D1	D3-D2	D4-D3	D4
	Inches	2.227	5.569	11.137	23.388

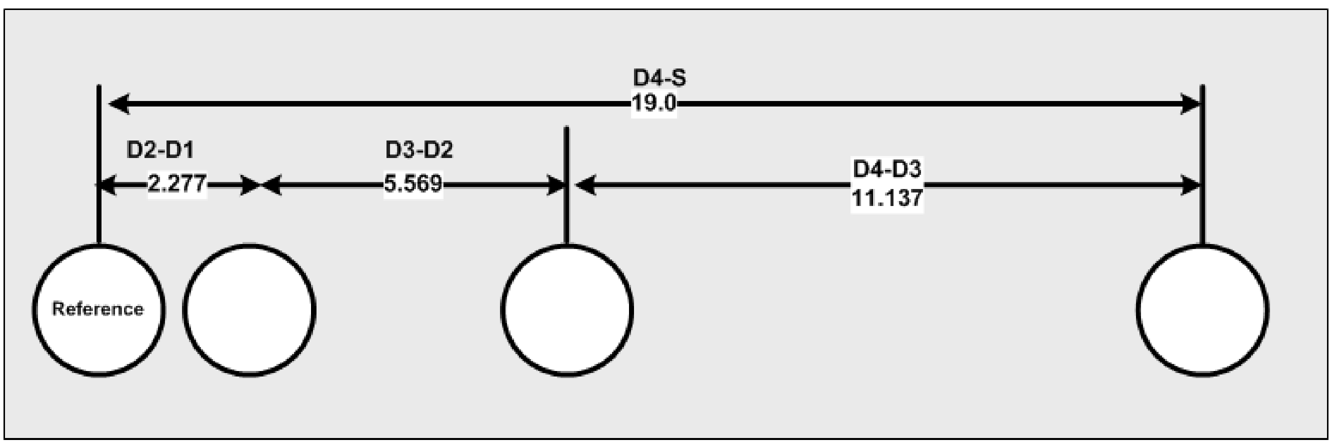

The antenna baseline spacing calculator expresses the Hybrid Mid-Phase geometry numerically. The four-element DF array is arranged as a linear sequence of antenna positions referenced to a fixed origin on the left side of the page. The elements labeled D2–D1, D3–D2, D4–D3, and D4 are positioned horizontally with increasing spacing determined by the design-anchor frequency and the wavelength-scaling model.

The spacing between D2 and D1 is 2.227 inches, the spacing between D3 and D2 is 5.569 inches, and the spacing between D4 and D3 is 11.137 inches. The total physical distance from D2 to D4 (the sum of the three spacings) is approximately 19 inches.

These distances correspond to the scaled half-wavelength values for the 18 GHz design anchor and provide the required phase progression across the aperture for CPU-based AOA and signal-parameter extraction.

The control panel provides the numerical framework for generating the array geometry. It contains the design-anchor frequency, the computed wavelength, the operating-frequency scale factor, and the half-wavelength phase distances for each antenna position. The panel also lists the unscaled physical distances and the final inter-element spacing values used to construct the array diagram. By adjusting the frequency or scale factor, the control panel updates the computed offsets and ensures that the array layout matches the required phase model for the selected operating band.

4. *Unwrapped* Phase Behavior

The unwrapped interferometer phase underpins all DF accuracy expressions. Figure 2, titled Unwrapped Phase for P, Q, R, and S, shows the unwrapped phase $\varphi = 2\cdot\pi\cdot D\cdot\sin(AoA)/\lambda$ for the four effective baselines after normalization and scaling. The hybrid mid-phase baselines P, Q, and R produce progressively steeper slopes, while the absolute outer baseline S generates the largest phase excursion across the field of view.

5. Local Phase Slope

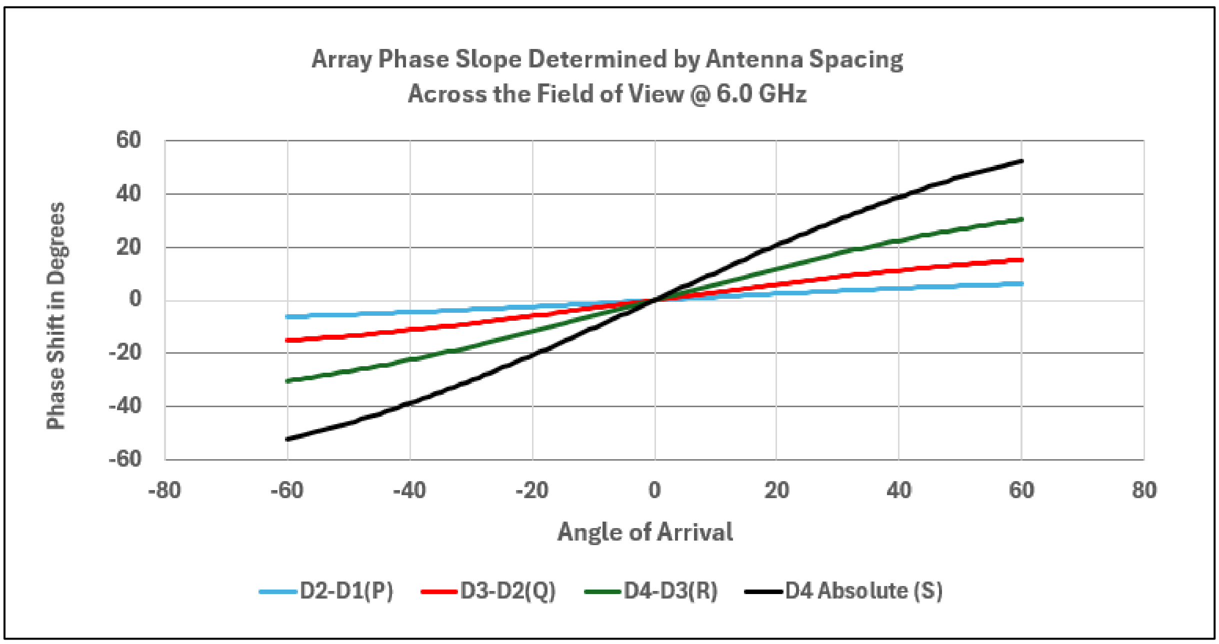

Figure 2 Local Phase Slope Magnitude for P, Q, R, and S

For illustration, the Excel worksheet uses the 6 GHz and 18 GHz frequencies for AOA phase-slope plots, matching the comparison frequencies used throughout the resolver analysis. MOD behavior is not shown in the main body; a representative MOD plot illustrating wrap spacing and baseline-dependent slope is included in Appendix A.

In this region, the physical antenna spacings represent only a moderate number of wavelengths, and the hybrid mid-phase baselines P, Q, and R remain electrically short enough to avoid wrap compression. The outer baseline S, although larger, still produces phase slopes that Excel can render cleanly without distortion.

As a result, the wrapped phase behavior exhibits minimal crowding, remains well separated across the full field of view, and provides a clear picture of baseline behavior without ambiguity. This band is therefore ideal for demonstrating wrap density, baseline separability, and the geometric relationships that drive resolver performance.

An AOA comparison at 6 GHz and 18 GHz is included to show how the resolver outputs behave when all embedded baselines remain fully stable. At these frequencies, the normalized phase-wrap behavior for the P, Q, R, and S baselines is well conditioned, and the hybrid mid-phase combinations do not degrade.

As a result, the four-element, three-element, and two-element resolver outputs track closely across the angle range, with minimal separation between configurations. This comparison provides the baseline reference case for resolver performance under ideal conditions, demonstrating the angle behavior before frequency-dependent degradation begins.

.

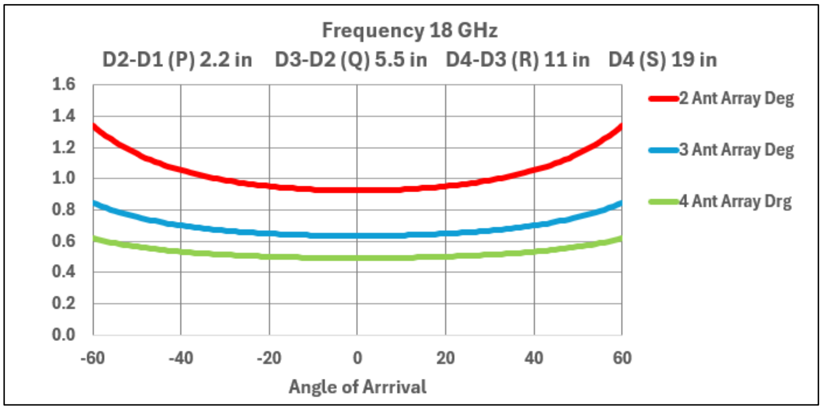

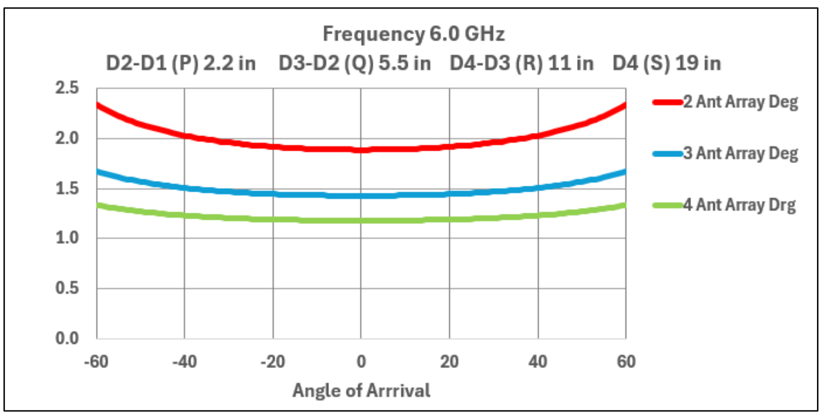

Figure 4 AOA Comparison at 6 GHz for 4-, 3-, and 2-Element Resolver Configurations

A second comparison plot shows array variance versus angle of arrival at 6 GHz, where all baselines remain stable across the angle range, supporting four-element resolver operation. At 18 GHz, the increased phase-slope variance reduces baseline conditioning and requires resolver transitions. These results illustrate the frequency-dependent baseline behavior that drives the resolver selection sequence described in the Summary Excel section.

This final figure links the numerical hybrid-resolver analysis to the antenna array's physical baseline behavior. The combined spreadsheet results and performance curves show how detector behavior, hybrid mid-phase formation, composite frequency-reference scaling, and resolver selection work together across the band.

6. AOA Resolvers Monte Carlo Simulation

Section 6, *AOA Resolvers Monte-Carlo Simulation*, demonstrates the array's tolerance to random phase mistracking between channels, showing that the Hybrid Mid-Phase AOA process remains stable and does not collapse under statistically applied phase error. Only the instantaneous accuracy of each individual Monte-Carlo trial varies; the underlying resolver behavior and array geometry remain unchanged.

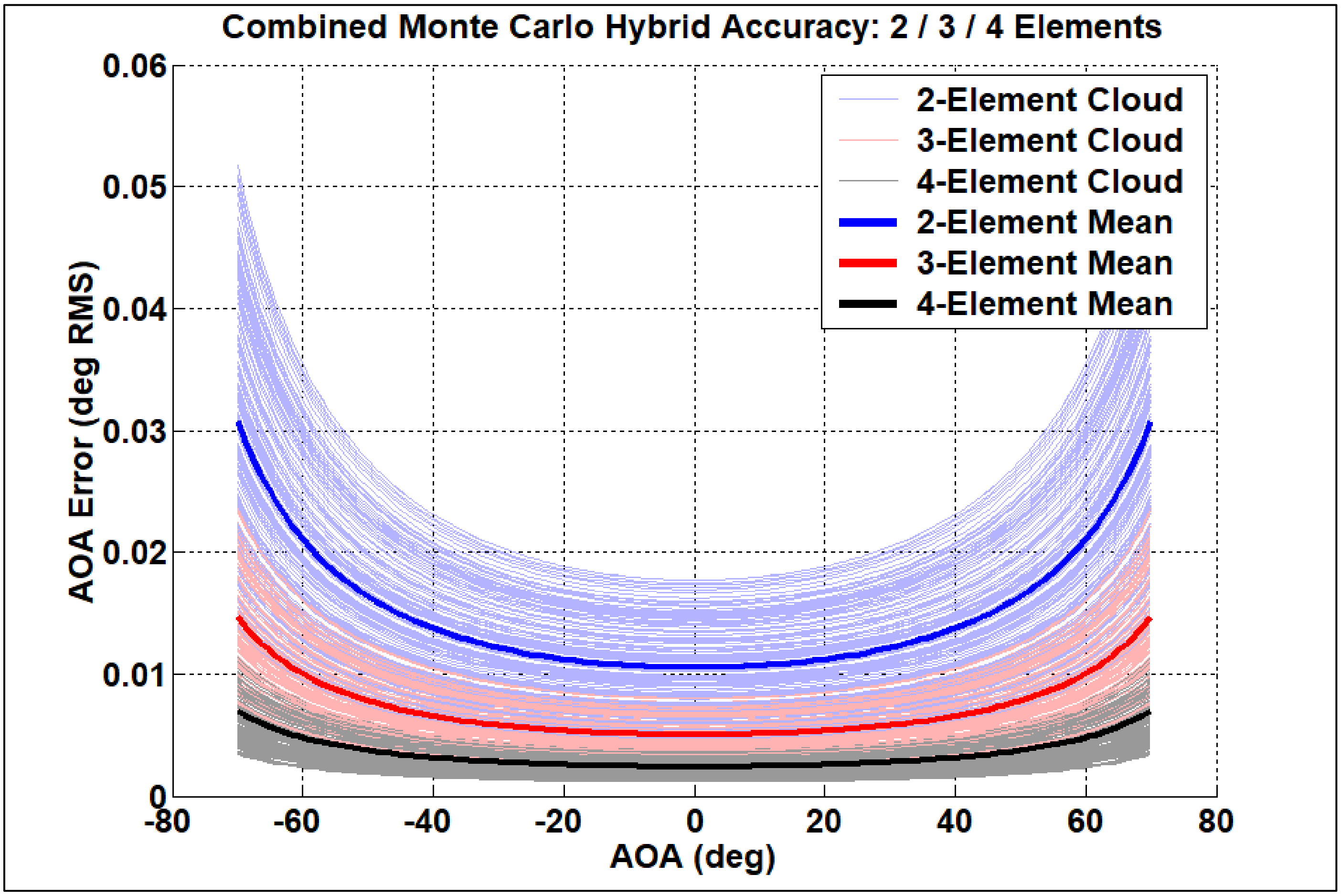

Figure 5 — Combined Monte-Carlo Hybrid Accuracy for 2-, 3-, and 4-Element Resolvers

7. Summary Excel

Across the operating band, the phase detectors follow the wrapped-phase behavior defined by the hybrid mid-phase baselines. Increased wrap density at higher frequency affects only the visualization and does not enter the resolver calculations. Frequency resolution is formed from two sources: the DLVA-derived IF characteristics and the instantaneous frequency estimate from the IFM. This estimate is combined with the DDS tuning word to form the composite frequency reference the LeGear FPGA uses. This reference is applied only for scaling and ADC protection and does not enter the resolver math.

The phase slope increases with frequency, causing the hybrid mid-phase value inside the FPGA to grow while the ADC input range remains fixed. The FPGA applies a frequency-based scaling factor derived from the composite frequency reference to keep the mid-phase output value within the ADC's dynamic range. The three hybrid paths feed the LeGear resolver function, producing linearized phase values that are digitized and combined after ADC conversion to form the final angle.

This processing ladder—phase-detector behavior, hybrid math, three resolver paths, composite-frequency scaling, ADC conversion, and angle reconstruction—maintains stable operation across the band. The Monte-Carlo accuracy curves quantify angle-error behavior for the four-element, three-element, and two-element resolvers and provide the statistical basis for resolver selection. As frequency increases and the longest baselines show increased phase-slope variance, the three-element resolver maintains lower error. At still higher frequencies, when only two embedded combinations remain reliable, the software selects the two-element resolver.

The Hybrid LeGear FPGA AOA resolver enables a self-referencing wideband interferometer architecture that requires no chamber measurements or calibration tables. The perfect-world Hybrid AOA values are known from interferometer geometry, and the operational Hybrid AOA values inherently contain the channel-to-channel RMS mistrack scaled to the DDS tuning word.

Because the Hybrid resolver collapses all baseline errors into a single observable angle bias, the difference between the perfect-world Hybrid AOA and the actual Hybrid AOA becomes the real-time correction factor.

The system is therefore self-correcting: it simply compares what it is to what it should be and applies the resulting bias directly, eliminating traditional calibration, providing a technical solution for YIG-filter RF preselectors, and removing the need for frequency-by-frequency mapping.

Appendix A — Illustrative MOD Response (FYI Only)

Figure A-1 shows a typical normalized MOD response for baselines P, Q, R, and S over a ±45° angle-of-arrival window at a mid-band frequency. This plot illustrates how baseline length controls phase-wrap spacing and slope: shorter baselines produce slower MOD variation with wider wrap spacing, while longer baselines produce faster variation and more frequent wraps. The MOD response is included solely to demonstrate the underlying phase-detector geometry that motivates the multi-baseline architecture.